



# Simple low-light image enhancement based on Weber–Fechner law in logarithmic space



Wencheng Wang <sup>a,\*</sup>, Zhenxue Chen <sup>b</sup>, Xiaohui Yuan <sup>c</sup>

<sup>a</sup> Weifang University, College of Information and Control Engineering, Weifang 261061, China

<sup>b</sup> Shandong University, College of Control Science and Engineering, Jinan 250061, China

<sup>c</sup> University of North Texas, College of Engineering, Denton, TX, 76207, USA

## ARTICLE INFO

### Keywords:

Logarithmic transformation  
Low-light image  
Non-uniform illumination  
Weber–Fechner law  
Color compensation

## ABSTRACT

In an environment with poor illumination, such as indoor, night, and overcast conditions, the image information can be seriously lost, which affects the visual effect and degrades the performance of machine systems. However, existing methods such as retinex-based method, dehazing model-based method, and machine learning-based method usually have high computational complexity or are prone to color distortion, noise amplification, and halo artifacts. To balance the enhancement effect and processing speed, this paper applies the Weber–Fechner law to the grayscale mapping in logarithmic space and proposed an adaptive and simple color image enhancement method based on the improved logarithmic transformation. In the framework, the brightness component is extracted from the scene of the low-light image using Gaussian filtering after color space conversion. The image is logarithmically transformed by adaptively adjusting the parameters of the illumination distribution to improve the brightness of the image. The color saturation is hence compensated. The proposed algorithm adaptively reduces the impact of non-uniform illumination on the image, and the enhanced image is clear and natural. Our experimental results demonstrate improved performance to the existing image enhancement approaches.

## 1. Introduction

Digital image processing is widely applied in industrial production, intelligent transportation, video surveillance, remote sensing monitoring, and other fields. It plays a significant role in the industry, human life as well as the military. However, under the condition of poor illumination [1–3], such as indoor, nighttime, and overcast conditions, the reflected light on the surface of the object is weak, and the image color obtained is distorted and contains much noise [4]. Especially in the fields of video surveillance, intelligent transportation, and automatic driving, which require constant intelligent analysis, low-light scenes such as dim light or night conditions affect not only the visual perception of human eyes but also the object recognition accuracy of subsequent machine systems and even lead to system paralysis [5,6]. A conventional infrared compensation scheme can obtain a clear image in a completely dark environment, but it will lose color information and form only a gray image with a large amount of noise. Therefore, under poor lighting conditions, enhancing image details and restoring color information to the full have become urgent requirements in various fields. Shown as the poorly lit images in Fig. 1, which are taken at night, indoors, or with backlighting, the non-uniform illumination makes some areas of the image too bright, while some areas are too dark.

Therefore, how to enhance the validity of the data and make the image more in line with human's visual perception while profiting the equipment's analysis is of great significance. For example, in a face recognition system, as Oloyede et al. [7] proposed, a new evaluation function was combined with the optimization algorithm based on metaheuristics, so as to select the best-enhanced face image automatically according to the linear combination of different key quantization indicators. In the field of underwater image enhancement, Hou et al. [8] proposed a new hue-preservation-based improvement method for underwater color images through the combination of hue-saturation-intensity (HSI) and hue-saturation-value (HSV) models. To measure yarn parameters more accurately, Wang et al. [9] proposed an adaptive grayscale improvement and linear region threshold segmentation algorithm, which enhanced the gray level contrast between the background and the yarn and improved the yarn hairiness recognition and measurement accuracy. In [10], aiming at the problem of low contrast in retinal fundus images, the author applies independent component analysis (ICA) to image enhancement and proposes an automatic retinal vascular segmentation method based on ICA, which can segment retinal vessels quickly and accurately. Pei et al. [11] put forward a color optimization algorithm for low-backlighted displays, and

\* Corresponding author.

E-mail address: [wwcwf@126.com](mailto:wwcwf@126.com) (W. Wang).

Kallel et al. [12] presented a new optimization algorithm for computed tomography (CT) scans using discrete wavelet transform with singular value decomposition (DWT-SVD) and adaptive gamma correction (AGC), which consistently produced satisfied contrast enhancement and preserved brightness.

However, these methods have many parameters that need to be adjusted, which tend to be over-enhanced in local areas with non-uniform illumination, and it is hard to keep the trade-off between the speed and performance. To solve the above problems, an image enhancement method based on Weber–Fechner law is proposed in this paper. This method applies local and global information to parameter adaptive adjustment and realizes fast enhancement through local logarithmic transformation, which can restore the low-light image into its natural scene of high contrast, vivid color, and rich details and can provide a valuable reference for the correction of non-uniform illumination images. Compared to previous work, our method offers the following contributions:

- It is a simple and effective strategy to map the gray levels of the image pixels to logarithmic space based on Weber–Fechner law;
- In the framework, the image is logarithmically transformed by adaptively adjusting the parameters of the illumination distribution to improve the brightness and has the compensation mechanism of color saturation;
- It applies local and global information to reduce the influence of non-uniform illumination on the image adaptively, and the enhanced image is clear and natural;
- This method does not need lots of datasets for training and can produce satisfying results with less computational complexity.

The rest of this paper is summarized as follows. Section 2 gives a brief introduction to related works. Section 3 presents the details of the model put forward in this paper. Qualitative and quantitative comparisons are reported in Section 4. We conclude our research in Section 5.

## 2. Related works

According to the working principle, the methods of low-light image enhancement are mainly divided into six categories: the gray mapping method, histogram equalization, frequency domain-based method, retinex-based method, dehazing model-based method, and machine learning-based method.

The gray mapping method is changing the gray values of an image through a mathematical function. For example, Drago et al. [13] designed an adaptive logarithmic function to map the image gray level, which can enhance the image dynamic range. Huang et al. [14] presented an algorithm that adaptively obtains gamma correction parameters in accordance with cumulative distribution function (CDF). Wang et al. [15] put forward an adaptive local gamma transformation for low-light image correction, which obtained the intensity component with a fast guided filter and built a local gamma transform function to improve the brightness of the image. This kind of method is simple; however, it has the limitation of robustness.

The histogram equalization (HE) method enhances the image by modifying the gray-level distribution. For example, Kim et al. [16] used block iteration to propose an adaptive histogram equalization (AHE) method. Kim [17] put forward the brightness-preserving bi-histogram equalization (BBHE) approach to perform HE on two sub-images after threshold division. As Celik and Tjahjadi [18] suggested, the nonlinear data mapping is carried out by a two-dimensional histogram of the input image. They also proposed a contextual and variational contrast enhancement (CVC) method to enhance a weak lighting image. Parihar and Verma [19] proposed a dynamic sub-histogram equalization algorithm based on entropy, which assigns a new dynamic range to each sub-histogram according to the number of entropy and gray levels. Gu et al. [20] applied a quality assessment model to the optimization of histogram parameters and Xu et al. [21] generalized the equalization



**Fig. 1.** Examples of different poor lighting conditions. (The first row shows images under night, indoor and backlit conditions; the second row displays the images enhanced by the proposed method).

model to effectively solve the problem of over-enhancement. Histogram equalization is simple and can be used in real-time scenes. However, it is easy to lose details caused by gray merging.

The method based on frequency domain analysis is to weaken the noise and enhance the contrast by processing the high and low-frequency information separately. For example, Zong et al. [22] put forward a contrast optimization algorithm according to the multiscale wavelet analysis, which enhanced an ultrasound image by setting a high-pass function to calculate wavelet coefficients. Loza et al. [23] put forward an adaptive contrast optimization algorithm through the local wavelet coefficients statistics, in which a nonlinear enhancement function was obtained for optimization by modeling. These kinds of methods are simple in principle and focus on contrast enhancement; however, they do not make full use of the true brightness of the image and risk of over-enhancement or under-enhancement.

Retinex is a color constancy-related theory created by Land and McCann [24]. Later, Jobson et al. [25] put forward the SSR (single scale retinex) method for image enhancement and further developed it into the MSR (multiscale retinex) method, MSRCR method (MSR with color restoration) [26,27], MSRPC method (MSR with chromaticity preservation) [28] and other conventional algorithms. In addition, Jang et al. [29] put forward an MSR algorithm on account of subband decomposition of fusion strategy. Wang et al. [30] proposed an algorithm called image naturalness preserved enhancement (NPE) through a bright-pass filter; it can both enhance the image contrast and avoid local over-enhancement. Fu et al. [31] put forward a weighted variational model by simultaneous reflection and illumination estimation (SRIE) on the observed image. After separating the reflection component and the luminance component with retinex theory [32], some researchers use a local nonlinear transformation model to enhance the luminance component to make the image look more natural and bright [33], introduce an enhancement adjustment factor [34], or adjust the enhancing degree of different luminance values to prevent noise amplification and color distortion [35,36]. Retinex-based algorithms have the advantages of clear physical meaning and easy implementation, but they have high computational complexity, and halo phenomena will occur in restored images.

In 2011, Dong et al. [37] inverted a low-light image to obtain a similar foggy image and then improved the image contrast by using dark/bright channel prior (DCP or BCP). Later, the algorithm is optimized by Zhang et al. [38], but the parameters in transmission estimation are directly obtained by experience, so the robustness is not satisfactory. Jiang et al. [39] adopted filters to process details and obtained transmission coefficient with a pyramid model; it can both increase the running speed and obtain better naturalness. On this basis, Pang et al. [40] introduced gamma transformation to enhance image contrast. Zhang et al. [41] put forward a real-time low-light image optimization algorithm through the combination of defogging and bilateral filtering, in which a joint bilateral filter is used to reduce the impact of noise after parameter estimation with DCP. Tao et al. [42] adopted

BCP with a convolutional neural network (CNN), and Park et al. [43] combined BCP with a retinex optimization method, all got satisfactory results. Hu et al. [44] put forward a fast low-light video optimization method through the combination of retinex and DCP theory, which incorporated scenario detection and edge and interframe compensation to improve the optimization performance. Low-light image has its own features after inversion, and the usage of dehazing method for low-light image processing is still not ideal for obtaining a satisfactory effect. How to improve the scientific rigor of transmission estimation is still a technical difficulty.

Machine learning-based method for image enhancement has just emerged recently. For example, Cepeda-Negrete et al. [45] established a set of fuzzy rules by combining three conventional enhancement methods with machine learning and adaptively chose the best enhancement algorithm for different image processing tasks. Lore et al. [46] adopted an auto-encoder in a low-light image optimization framework and trained the characteristics of different low-light images to achieve self-adaptive enhancement and denoising by deep learning. Shen et al. [47] combined the MSR method with CNN and put forward an optimization method for low-light image enhancement. Tao et al. proposed a framework to learn low-light images with different kernels, and multilevel feature graphs were used to generate enhanced images [48]. Park et al. [49] put forward a convolutional automatic encoder to process image data for noise reduction during the brightness optimization and achieved a good effect. Enlightened by the approach of image fusion, Cai et al. [50] put forward an algorithm to train a single image intensifier with CNN on a large-scale multi-exposure image dataset, and produce an improved image from a series of images. Gharbi et al. [51] designed a deep bilateral learning (DBL) framework, which realized real-time processing of image enhancement. Wang et al. [52] designed a global illumination-aware and detail-preserving network (GLADNet), which uses a CNN to reconstruct details based on global a priori knowledge and original input images. This kind of method has a good enhancing effect, but its computational model requires too much time or too many expensive resources for training.

According to Weber-Fechner law, there is a certain relationship between mental perception in the human visual system and the true quantity of light intensity [53]. The reason why human eyes can distinguish different objects is that those objects have different reflectance, thus forming a contrast in the brightness and color between objects. To cause visual perception differences, the same stimulus difference must reach a certain proportion, which is the difference threshold. The difference threshold is proportional to the standard stimulus, and the proportion coefficient is a constant  $\lambda$ , which is expressed by  $\lambda = \Delta I/I$ . Therefore, if the smallest sensible difference is taken as the sensory quantity unit, the psychological quantity will be increased by one unit for each additional difference threshold. Let  $f(x)$  be a function of the change in visual perception with the increase in light intensity, then  $f'(x)$  is a function of subjective perception with the increase in the stimulus increment  $\Delta x$ . According to Weber-Fechner law, then:

$$f'(x) = \lambda \times \frac{dx}{x}, \quad (1)$$

Taking the integral of both sides:

$$\int f'(x)dx = \lambda \times \int \frac{1}{x}dx, \quad (2)$$

The integral results are as follows:

$$f(x) = \lambda \times \ln x + C, \quad (3)$$

When  $f(x) = 0$ , then,  $C = \lambda \times \ln x'$ . The factor  $x'$  is an absolute threshold, indicating that the stimulus under this threshold intensity causes a perceptual difference of 0, that is, no perceptual change. Combining the above formulas, we can obtain:

$$f(x) = \lambda \times (\ln x - \ln x'), \quad (4)$$

If the absolute threshold is set to 1 as the measuring unit, then  $\ln x' = 0$ , and Eq. (4) will change to:

$$f(x) = \lambda \times \ln x, \quad (5)$$

It can be seen from the formula that the subjective sensation of the HVS  $f(x)$  and the intensity of light  $x$  are logarithmic. If the pixels of the image are transformed into logarithmic space, the current value of the logarithmic domain of the global image is processed to get the enhanced image.

### 3. Framework of the proposed method

The overall algorithm framework in this paper is shown in Fig. 2.

#### 3.1. Color space conversion

For color images, RGB color space is limited to distinguishing chroma and brightness information. If the three channels (R, G, B) are corrected directly in RGB color space, not only can color distortion easily occur but also the complexity of the calculation increases. So, we convert the image to Lab color space for processing. In this space,  $L$  represents the color brightness; positive values of  $a$  represent redness, and negative values represent greenness; positive values of  $b$  represent yellowness, and negative values represent blueness.

The conversion from RGB to XYZ color model is as follows:

$$\begin{bmatrix} X \\ Y \\ Z \end{bmatrix} = \begin{bmatrix} 0.412453 & 0.357580 & 0.180423 \\ 0.212671 & 0.715160 & 0.072169 \\ 0.019334 & 0.119193 & 0.950227 \end{bmatrix} \begin{bmatrix} R \\ G \\ B \end{bmatrix}, \quad (6)$$

Then, XYZ space is converted to Lab space by:

$$\begin{cases} L = 116f(Y/Y_n) - 16 \\ a = 500[f(X/X_n) - f(Y/Y_n)], \\ b = 200[f(Y/Y_n) - f(Z/Z_n)] \end{cases} \quad (7)$$

$$f(t) = \begin{cases} t^{1/3} & t > (\frac{6}{29})^3 \\ \frac{1}{3}(\frac{29}{6})^2t + \frac{4}{29} & otherwise \end{cases}, \quad (8)$$

In these two formulas,  $L$ ,  $a$ , and  $b$  are the three channels' values in the Lab color space.  $X$ ,  $Y$ , and  $Z$  are calculated after converting to XYZ color space. Generally, the values for  $X_n$ ,  $Y_n$ , and  $Z_n$  are 95.047, 100.0, and 108.883, respectively. After converting RGB to Lab color space, the image examples of each component are displayed in Fig. 3.

#### 3.2. Illumination estimation

To estimate the illumination information from an image, the  $L$ -component image is blurred and smoothed with the hypothesis that the illumination usually changes slowly in local regions. The blurred image sets the current pixel to the mean of the pixels in its neighborhood, as shown in Fig. 4. The center pixel value in the left image is 4. After summing the values in its  $3 \times 3$  neighborhood, the average value 1.6 will replace the center pixel, as in the right image. This simple average blurring is unreasonable because an image is continuous in space, which also means that the closer the distance, the higher the weight should be. Although bilateral filtering and guided filtering are often used for image blurring, those are the edge-preserving filters. Therefore, the Gaussian function was used in the weighted average method for blurring. If the two-dimensional template size is  $m \times n$ , the corresponding Gaussian function of the elements  $(x, y)$  on the template is as follows:

$$G(x, y) = \frac{1}{2\pi\sigma^2} e^{-\frac{(x-m/2)^2+(y-n/2)^2}{2\sigma^2}}, \quad (9)$$

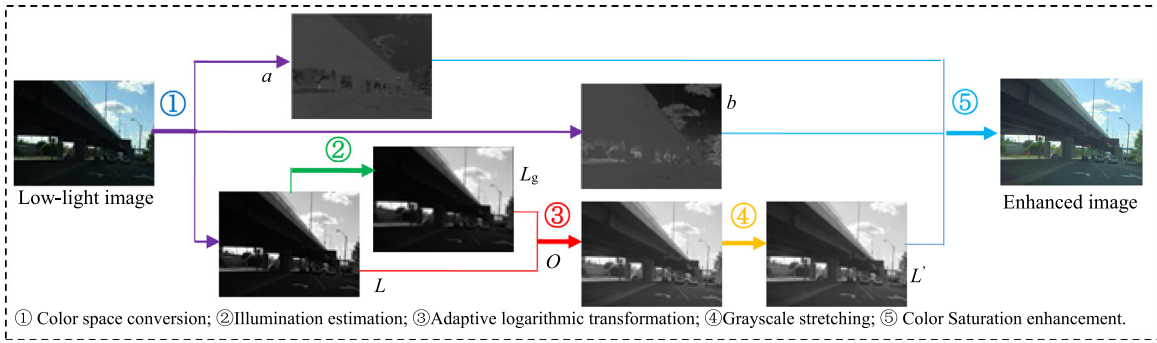


Fig. 2. Proposed algorithm framework.

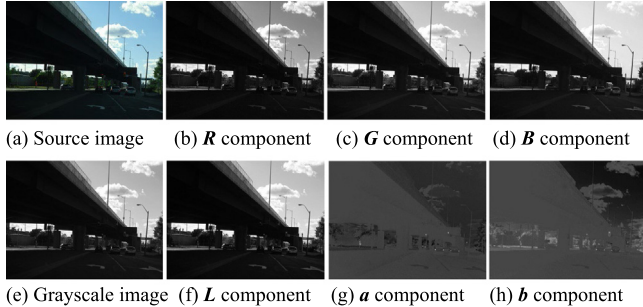


Fig. 3. An example of converting RGB color space to lab color space.

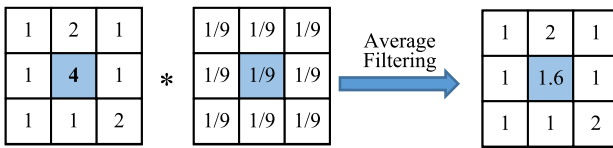


Fig. 4. Average filtering.

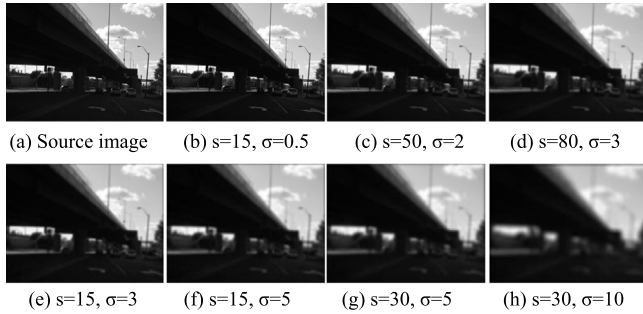


Fig. 5. Changes in image blurring with different parameters.

where  $\sigma$  is the normal distribution's standard deviation. The larger the value of  $\sigma$ , the more blurred the image is.

In two-dimensional space, the surface contour generated by this formula is a concentric circle with a normal distribution from the center, and its weight distribution is shown in Fig. 5. The process of Gaussian filtering is taken as the convolution of the Gaussian function and the original image, and the illumination component's estimated value can be obtained. The formula is as below:

$$L_g(x, y) = L(x, y) * G(x, y), \quad (10)$$

where  $L(x, y)$  is the input image,  $L_g(x, y)$  is the estimated illumination component,  $G(x, y)$  is the Gaussian filter and  $*$  denotes convolution.

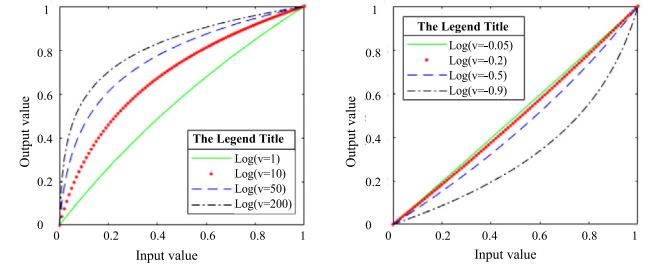
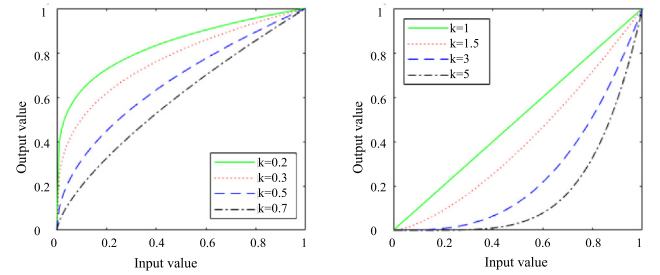


Fig. 6. Logarithmic transformation curves.

Fig. 7. The output curves with changing  $k$ .

In this way, each pixel value is replaced by the weighted average of its neighborhood. The farther away the neighbor pixels are from the original pixels, the smaller their weights. In our experimental, we set the same size of  $m$  and  $n$  with the parameter  $s$ . Fig. 6 is the result of Gaussian filtering with three groups of parameters ( $[s = 15, \sigma = 0.5]$ ,  $[s = 50, \sigma = 2]$ ,  $[s = 80, \sigma = 3]$ ,  $[s = 15, \sigma = 3]$ ,  $[s = 15, \sigma = 5]$ ,  $[s = 30, \sigma = 5]$ ,  $[s = 30, \sigma = 10]$ ).

On the basis of both the efficiency and the effect of the operation, the paper adopts Gaussian filtering to extract the illumination component with a filter window size of  $15 \times 15$  pixels and  $\sigma$  of 0.5.

### 3.3. Adaptive logarithmic transformation

Logarithmic transformation is mainly used to expand the low grayscale values of the image and compress the high grayscale values of the image to achieve image enhancement, and it has the following standard forms:

$$O = c \cdot \log_{v+1}(1 + v \cdot L) \quad r \in [0, 1], \quad (11)$$

where  $O$  is the corrected image in the range of  $[0, 1]$ ,  $L$  is the source image,  $c$  is the gain adjustment parameter and the base value of  $v + 1$  is the control parameter. When  $v$  is greater than 1, the image as a whole will be brightened, and when  $v$  is less than 1 and greater than 0, the

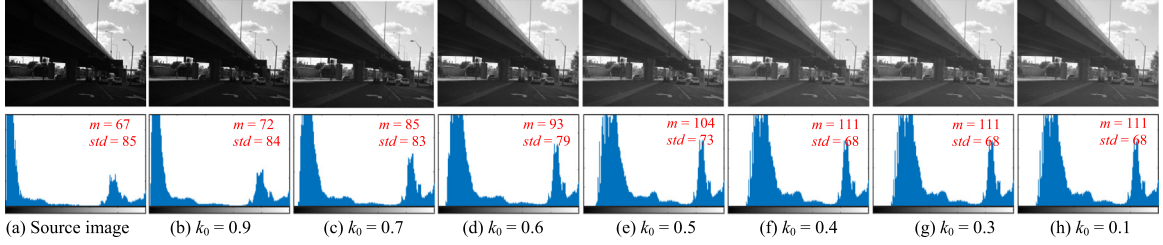


**Fig. 8.** Samples of the enhancement effects with varying  $k_0$ .

image as a whole will be darkened. Suppose  $c = 1$ . The corresponding transformation curves when  $v$  is set to 1, 10, 50, 200, or  $-0.05$ ,  $-0.2$ ,  $-0.5$ , and  $-0.9$  are shown in Fig. 6.

As seen from Fig. 6, when  $v$  is greater than 0, the base number is large, and the enhancement of the low grayscale values is strong. When the image is globally dark or glossy, the algorithm can achieve satisfactory results by adjusting  $v$ , but if one image has under-exposure and normal exposure areas, the same parameter will easily cause over-enhancement. Therefore, we propose an algorithm that changes with the local information of the image to obtain a more satisfactory result by the following formula:

$$O = \exp(k \cdot \ln(L_g / L_{\max} + \xi)), \quad (12)$$

where  $L_g$  is the estimated illumination image from  $L$ ,  $k$  is the adjustment factor,  $L_{\max}$  is the maximum value of  $L$ , and  $\xi$  is the compensation factor that is set to a small value ( $\xi = 0.001$ ) to avoid a zero value in the logarithmic operation. Generally, for the areas with lower illumination, strong correction should be implemented, so the value of  $k$  should be small, while for the images with better contrast, the value of  $k$  should be large. The output curves with changes in  $k$  are shown in Fig. 7(a).

To enhance the low-light area adaptively according to the illumination distribution, this paper takes the  $k$  value as a parameter that varies with the illumination component of the scene and designs a parameter selection strategy based on the combination of the global brightness and local brightness, which adaptively adjusts the optimization function following the image illumination distribution. The parameter  $k$  can be expressed as follows:

$$k = \max[(L + L_m + L_{\max})/3, k_0], \quad (13)$$

where  $L_m$  and  $L_{\max}$  are the mean and the maximum value of  $L$ , respectively, and  $k_0$  is the control factor. The output images and corresponding histograms varying with different values of  $k_0$  are shown in Fig. 8 ( $k_0$  is set to 0.1, 0.3, 0.4, 0.5, 0.6, 0.7, and 0.9 in the subfigures). In which  $m$  represents the mean and  $std$  represents the standard deviation.

As seen from Fig. 8, with decreasing  $k_0$ , the pixels with small values are enhanced, and the pixels with large values are suppressed, the image dynamic range is compressed, the overall image brightness is enhanced, but the contrast is weakened. However, when  $k_0 < 0.4$ , the brightness value of the image does not change with the change of  $k_0$ . In practice,  $k_0$  is set to 0.5.

#### 3.4. Grayscale stretching

To alleviate the problem of gray value concentration, we use a grayscale stretching function to improve the image; that is, through a simple linear operation, we expand the image grayscale and improve the dynamic range by image processing.

Assume that  $O(x, y)$  is the input image; its minimum grayscale  $A$  and maximum grayscale  $B$  are defined as follows:

$$A = \min[O(x, y)], \quad B = \max[O(x, y)], \quad (14)$$

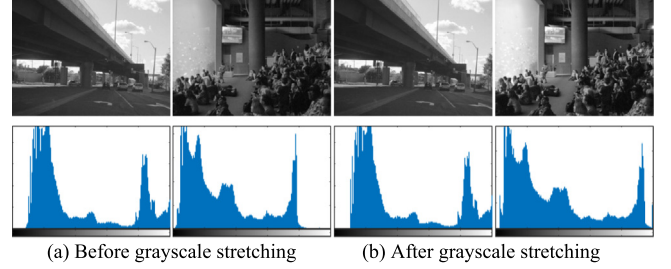


**Fig. 9.** Images and histograms before and after grayscale stretching.

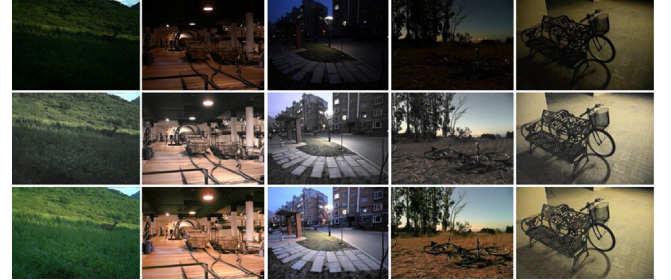


**Fig. 10.** Comparison of two different restoration methods. (The first row contains low-light images; the second row contains the images obtained without color compensation; the images in the third row are obtained with our method).

Set the darkest 0.5% of the input image to  $C$  and the brightest 0.5% to  $D$ . The dynamic range  $[C, D]$  is linearly mapped to  $[A, B]$ , and the final image  $L'(x, y)$  is as follows:

$$L'(x, y) = \frac{(D - C)}{B - A} O(x, y) + \frac{BC - DA}{B - A}, \quad (15)$$

As seen from Fig. 9, the image dynamic range is expanded after implementing this algorithm, which can enhance the image contrast while retaining the details of the areas with too high and too low brightness values.

#### 3.5. Color saturation enhancement

According to the principle of mutual conversion between Lab and RGB color space, and keeping  $a$  and  $b$  components unchanged, combining with the enhanced  $L'$  component, Eqs. (16) and (17) can be used to convert Lab to RGB color space.

$$\begin{cases} Y = Y_n f^{-1}\left(\frac{1}{116}(L' + 16)\right) \\ X = X_n f^{-1}\left(\frac{1}{116}(L' + 16) + \frac{1}{500}a\right), \\ Z = Z_n f^{-1}\left(\frac{1}{116}(L' + 16) - \frac{1}{200}a\right) \end{cases} \quad (16)$$

$$f^{-1}(t) = \begin{cases} t^3 & t > \frac{6}{29} \\ 3\left(\frac{6}{29}\right)^2(t - \frac{4}{29}) & otherwise \end{cases} \quad (17)$$

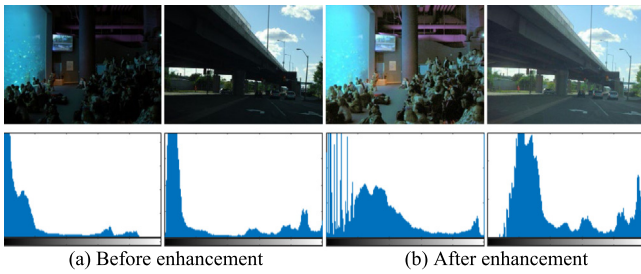


Fig. 11. Examples of images with histograms before and after enhancement.



Fig. 12. Some of the experimental images.

However, after converting to RGB space using the general method above, the image will have a lower color saturation. In Fig. 10, the first row contains the low-light images, and the second row contains the enhanced results without saturation compensation, which shows that the image appears to be insufficiently colored and the color saturation in the original image is slightly lost.

To maintain the color saturation of the output image consistent with that of the input image, we adopt the following method, which is expressed as:

$$\begin{cases} R' = \omega \times [(L'/L) \times (R + L) + R - L] \\ G' = \omega \times [(L'/L) \times (G + L) + G - L], \\ B' = \omega \times [(L'/L) \times (B + L) + B - L] \end{cases} \quad (18)$$

where  $\omega = 0.5$  and  $R, G, B$  are the three channels of an image, respectively.

As seen from the third row of Fig. 10, the color saturation and contrast of the image obtained by Eq. (18) are better than those with Eqs. (16)–(17). The samples of the original image and its enhanced image are displayed in Fig. 11.

#### 4. Experimental results analysis

To verify the effectiveness of the method, we built an experimental platform for testing. The computer processor used was i7-6700@3.4 GHz, and MATLAB was used as the simulation software. The images used for testing involve urban scenery, natural scenery, indoor images, etc. Some original low-light images are displayed in Fig. 12. The common features of the images are low brightness, non-uniform illumination, and a wide dynamic range. Some samples are shown in Fig. 13. The odd-numbered rows contain the original images, and the even-numbered rows contain the enhanced images. It can be seen that the low illumination area is enhanced and the high illumination area is suppressed after implementing the algorithm, and the enhanced image color is natural and the details are clear. This finding shows that the method can adaptively weaken the influence of non-uniform illumination on the image quality. In the following section, we will compare the results with those of mainstream algorithms from subjective and objective perspectives.

#### 4.1. Subjective evaluation

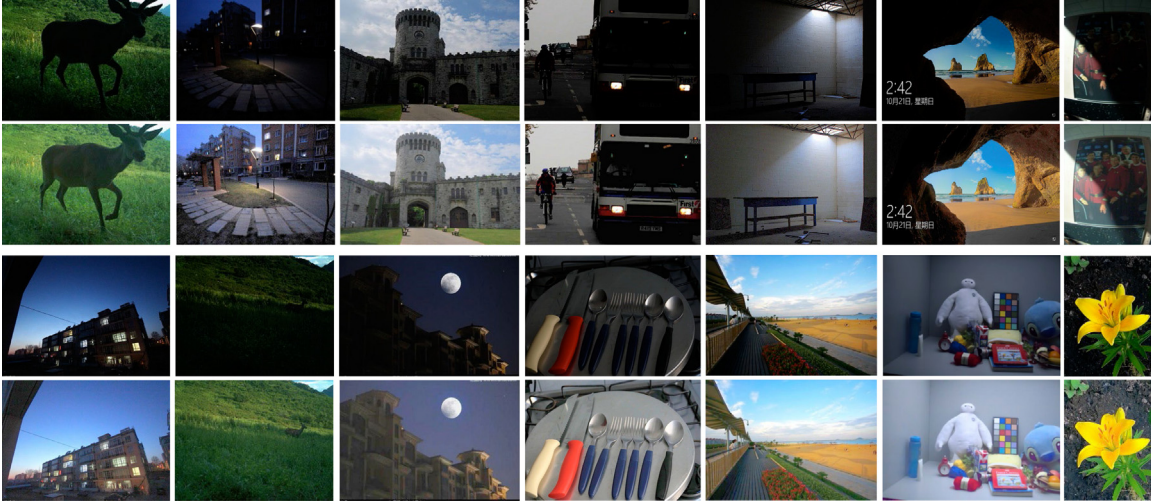
(1) Comparing the proposed method with the traditional image enhancement methods.

Fig. 14 indicates the experimental results of our method and some traditional methods. Fig. 14(a) is the original image. Fig. 14(b)–(h) are the enhanced images of a linear transformation (LT), HE, AHE, homomorphic filtering (HF), wavelet transform (WT), the retinex method (RM) and our method, respectively, and the enlarged areas corresponding to the rectangular box in Fig. 14(a) are shown in the second, fourth and sixth rows. As seen from the figure, the images processed by different methods have different degrees of change compared with the original image. Fig. 14(c) and (g) have a significantly enhanced visual contrast, and the details have become prominent. However, the tone has shifted, especially the serious halo noise in Fig. 14(g), leading to poor visual quality. For Fig. 14(e) and (f), although the overall tone is not shifted, the improvement in the details is insufficient and the image is even blurred. Fig. 14(b), (d), and (h) have better visual effects, but the LT method leads to an over-enhancement of the bright area of the image, while the color in the AHE image is dark. By contrast, the proposed method has improved the performance of images both in color and contrast, and the visual effect is better than that of other methods.

(2) Comparing the proposed algorithm with some state-of-the-art (SOTA) methods.

In this section, five images are randomly selected as the samples to show the advantages of the proposed algorithm by comparing it with some SOTA methods. The results are shown in Fig. 15, where (a) contains the low-light images and their enlarged regions. Fig. (b)–(i) are the processing results of AGCWD [54], SRIE [31], IBOOST [55], L2UWE [56], KinD [57], RetinexNet [58], FCCE [59] and our method, respectively. Compared with the original image, the clarity and contrast of the processed image are greatly improved, and a better enhancement effect is obtained. For these images, the RetinexNet method enhances the brightness of the image as a whole, but the tone deviates seriously. The AGCWD method and the FCCE method have a low enhancement degree, and the noise of the dark area is enhanced. In particular, the AGCWD method is limited to restoring the details from severely dark regions. The IBOOST method and the L2UWE and the KinD method can enhance the intensity of the image well. However, the IBOOST method leads to image over brightness, while the L2UWE method has an obvious hole effect in some regions, and the KinD method will cause the edge of the image to blur. Compared with the other methods, the SRIE method and our method maintain a balance of color and brightness information, and the visual effects are better than those of the above methods. However, the results of SRIE are not uniform enough for the areas between brightness and dark, and the overall effect of SRIE is not as good as that of our method. Comparing the local details of the content in the image box, there is noise caused by over-enhancement of the IBOOST, insufficient enhancement by FCCE and SRIE, there is over-enhancement of the IBOOST, noise amplification by AGCWD and RetinexNet, and shadows with the L2UWE method and KinD method in the local area. The proposed method can emphasize details without over-enhancement and without amplifying the noise in the dark area and can obtain better clarity, contrast, and image color.

We also adopted the low-light/normal-light image pairs of the IEC database for the experiment [60]. Some experimental results are indicated in Fig. 16, where (a) contains the original images and (b) contains corresponding reference images, which are under-exposed images and properly exposed images using a single shot, respectively. Fig. 16(c)–(i) are the processing results of AGCWD, SRIE, IBOOST, L2UWE, RetinexNet, FCCE, and our method, respectively. From those images, it can be seen that the outputs of AGCWD, SRIE, L2UWE, and FCCE are all having lower brightness than the reference image. To the results of RetinexNet, the hue has shifted. Only the images from IBOOST and our method are very similar to the reference image both



**Fig. 13.** Some of the experimental results before and after enhancement.

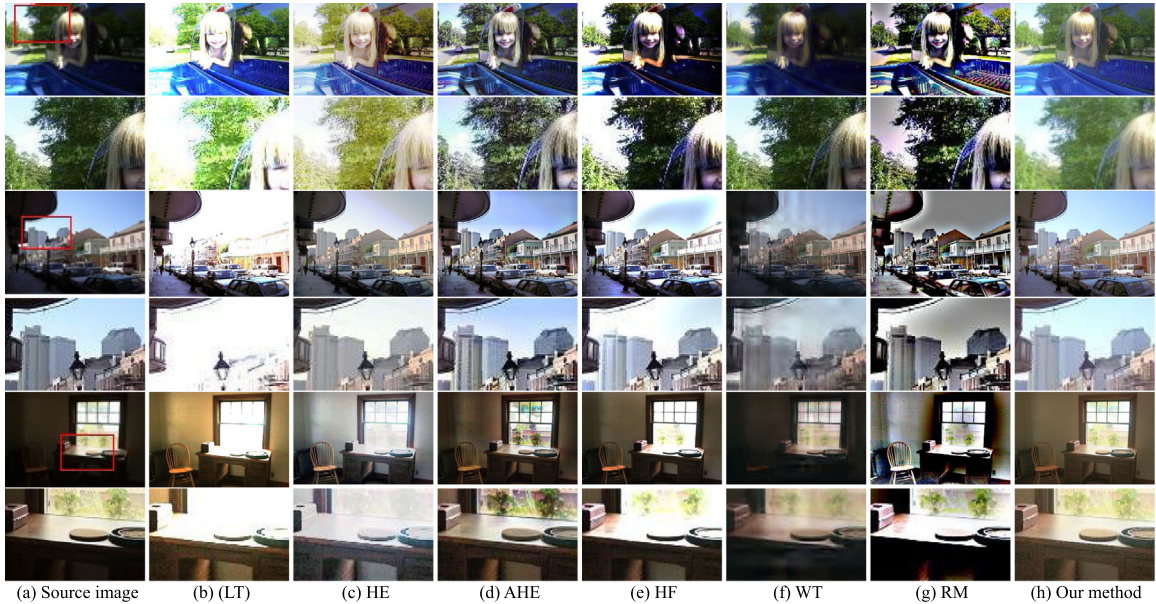


**Fig. 14.** Comparisons of conventional image enhancement methods.

in brightness and color, especially the latter is better. Fig. 17(a)–(h) are the corresponding polar hue map of Fig. 16(b)–(i). Among them, red, green, and blue curves represent the value distribution of three color components. It is easy to see that our method is the closest to the reference image, which is consistent with the visual perception in Fig. 16.

In addition, to further compare the processing effects of different algorithms, several synthesized images are also used in the experiment. As shown in Fig. 18, the (a) images are actual images with normal illumination, the (b) images are the low-light images from (a) processed by a gamma transform ( $\gamma = 2$ ), and (c) are images enhanced with our method. The experimental results show that our new algorithm can enhance the brightness of the low illumination region and suppress the brightness of the high illumination region adaptively, and the visual effect is consistent with the actual images. In Fig. 19, the proposed method was also compared with some existing methods, in which (c)–(h) are images that have been enhanced by different methods. We can see that the enhanced results of this method are the most similar to the original image in terms of the gray-level distribution and structure, and its comprehensive performance is far superior to that of other methods; it achieves the best results.

#### 4.2. Objective evaluation

Because different methods have different emphases, subjective evaluation is inevitably one-sided. Therefore, objective evaluation criteria such as image quality assessment

(IQA) and computational complexity are used to further measure the performance of different methods. IQA can be categorized as no-reference IQA and reference IQA.

##### (1) No-reference IQA

In this paper, the FGI (fusion of gradient information) [61] and NIQE (natural image quality evaluator) [62] were adopted as no-reference IQA metrics to measure the performances of the different methods. According to the theory of FGI and NIQE, the higher the FGI value is, the richer the details. For the NIQE, a smaller value is better.

To show the universality of the proposed method, the images from the IEC database [60], the LDR database [63], the LoL database [58], the PMEA database [64], and our self-built database were experimentally tested, the total number of the images is 986. Table 1 shows the objective evaluation results of methods AGCWD, SRIE, IBOOST, L2UWE, FCCE, RetinexNet, and our method, in which the results of

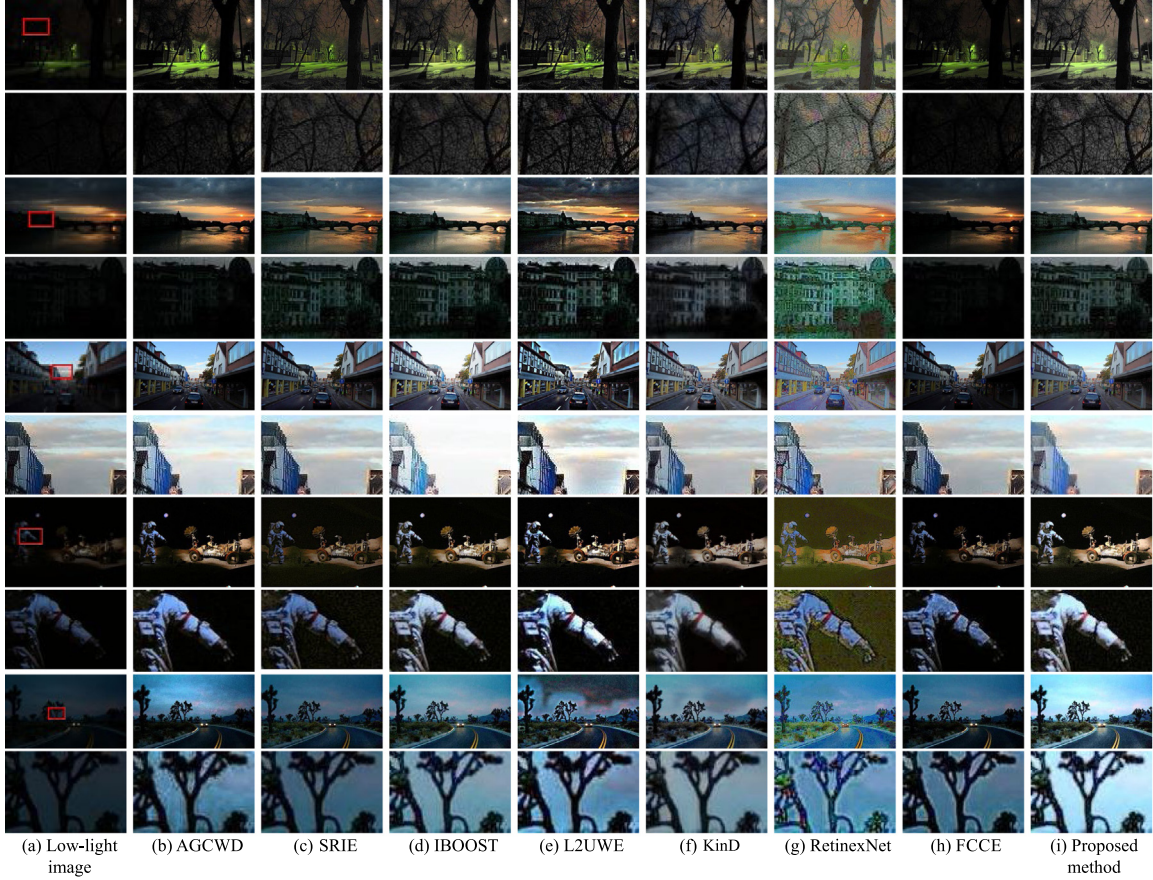


**Fig. 15.** Comparisons of several existing methods using non-reference images.

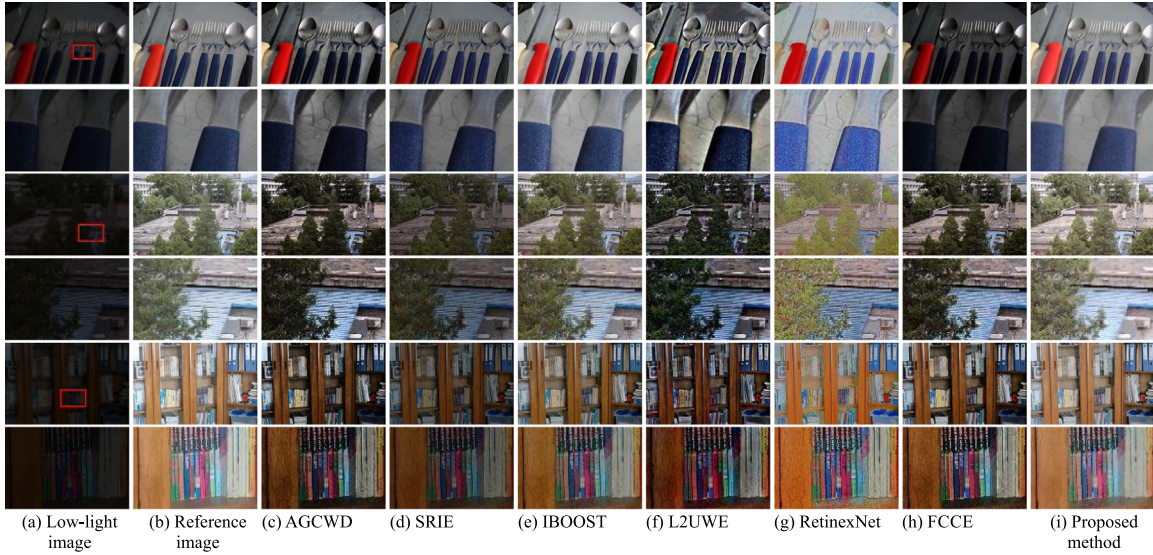


**Fig. 16.** Comparisons of several existing methods using image pairs of IEC database.

the same database's images were averaged as the final result, and the numbers parenthesis are standard deviation.

The method proposed in this paper can perform 7/8 the best or second-best values on the metrics of FGI and NIQE. Especially to the metric of NIQE, it obtained the three best out of the four databases. The values of all two indexes of our method are better than those of the other algorithms when applied to the LDR database and the PMEA database. To the database of LoL, the SRIE method get the

best performance on both FGI and NIQE. On the IEC database, the performance of the method is better than other methods in terms of the NIQE. Overall, the results show that among the twelve groups of data, our method outperforms the other algorithms on eight groups of data, indicating that our method performs better overall than the others.

#### (2) Reference IQA

The MSSIM (multi-scale structural similarity) [65], LOE (lightness order error) [66], and PSNR (peak signal-to-noise ratio) indexes are

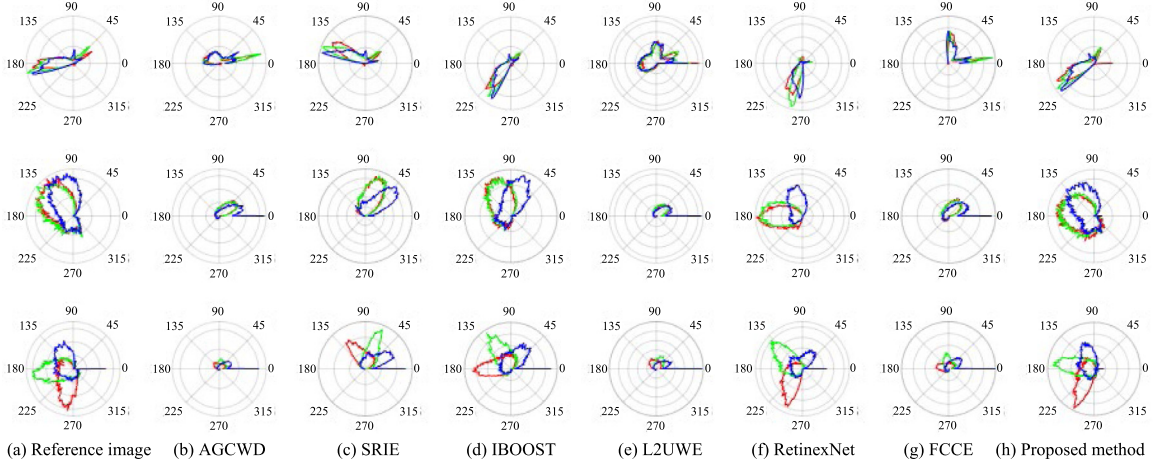


Fig. 17. Polar tone maps of images in Fig. 16.

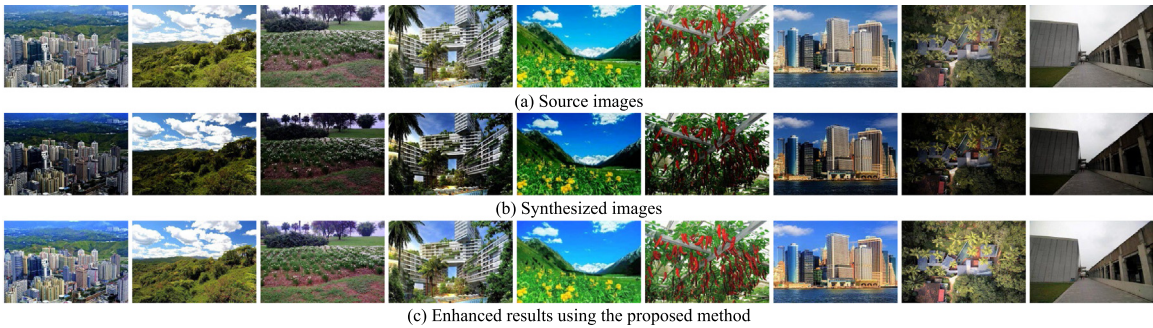


Fig. 18. Samples of synthesized image enhancement using the proposed method.

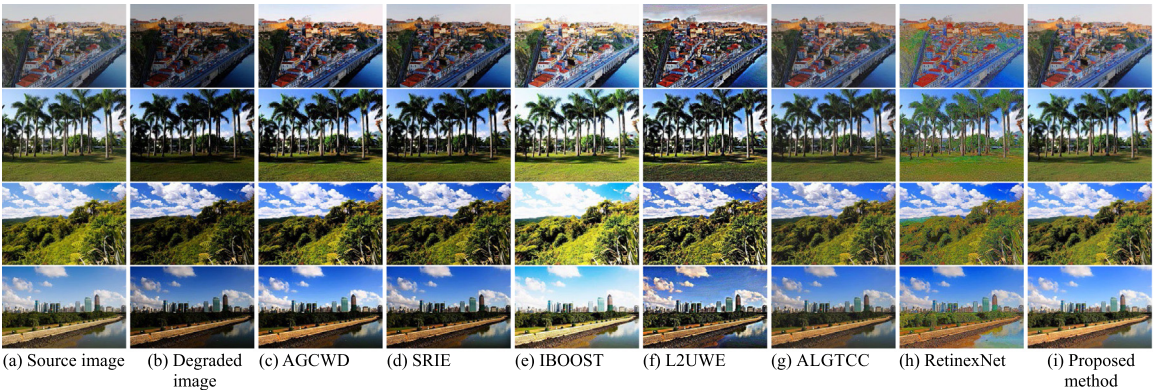


Fig. 19. Comparison of several state-of-the-art methods using the synthetic images.

Table 1

Objective quality evaluation on images from four databases enhanced with different methods. (The best result is bolded and the second best one is underlined).

Metric	Datasets	AGCWD	SRIE	IBOOST	L2UWE	RetinexNet	FCCE	Ours
FGI	IEC	0.465 (0.061)	0.353 (0.091)	0.401 (0.080)	0.532 (0.068)	<b>0.326</b> (0.059)	0.451 (0.064)	<u>0.352</u> (0.076)
	LDR	0.532 (0.071)	0.473 (0.073)	0.478 (0.070)	0.578 (0.048)	0.430 (0.067)	0.509 (0.072)	<b>0.387</b> (0.105)
	LoL	0.420 (0.089)	<b>0.227</b> (0.087)	0.355 (0.088)	0.381 (0.156)	0.295 (0.055)	0.407 (0.069)	0.368 (0.110)
	PMEA	0.514 (0.053)	0.482 (0.056)	0.459 (0.076)	0.570 (0.037)	<u>0.418</u> (0.069)	0.501 (0.047)	<b>0.379</b> (0.093)
NIQE	IEC	3.866 (0.920)	<u>3.668</u> (0.951)	3.838 (0.994)	3.977 (0.909)	4.944 (1.114)	3.955 (1.211)	<b>3.548</b> (0.929)
	LDR	3.347 (0.926)	<u>3.223</u> (0.864)	3.670 (1.132)	3.366 (0.889)	4.366 (1.147)	3.509 (1.185)	<b>3.078</b> (0.824)
	LoL	4.351 (1.198)	<b>3.602</b> (0.979)	3.977 (1.093)	4.066 (1.177)	6.512 (2.082)	4.202 (1.409)	<u>3.908</u> (1.090)
	PMEA	3.344 (1.012)	<u>3.181</u> (0.906)	3.410 (1.097)	3.443 (0.954)	4.461 (1.451)	3.225 (0.753)	<b>3.153</b> (1.010)

**Table 2**

Objective quality evaluation on images of Fig. 16 (The best result is bolded and the second best one is underlined).

	Metrics	AGCWD	SRIE	IBOOST	L2UWE	RetinexNet	FCCE	Ours
Group1	MSSIM	0.876	0.939	<b>0.955</b>	0.761	0.727	0.863	<b>0.970</b>
	LOE	534.850	266.717	<b>167.166</b>	926.551	893.877	129.889	<u>206.075</u>
	PSNR	14.792	<u>20.671</u>	19.422	17.204	13.935	12.325	<b>21.881</b>
Group2	MSSIM	0.846	0.738	<b>0.886</b>	0.810	0.649	0.844	<u>0.882</u>
	LOE	718.598	344.957	<u>322.053</u>	674.256	851.689	497.845	<b>279.406</b>
	PSNR	14.361	10.519	<u>17.931</u>	10.429	16.027	13.149	<u>19.657</u>
Group3	MSSIM	<u>0.955</u>	0.843	0.954	0.879	0.792	0.911	<b>0.960</b>
	LOE	564.459	<u>346.458</u>	<b>284.519</b>	622.859	1202.721	380.237	359.033
	PSNR	16.157	9.131	14.164	9.747	<u>16.831</u>	12.204	<b>21.705</b>

**Table 3**

Objective quality evaluation on images from two databases enhanced using different methods (The best result is bolded and the second best one is underlined).

Metric	Dataset	AGCWD	SRIE	IBOOST	L2UWE	RetinexNet	FCCE	Ours
MSSIM	IEC	0.874 (0.100)	0.926 (0.077)	<u>0.946</u> (0.095)	0.752 (0.083)	0.736 (0.092)	0.846 (0.161)	<b>0.952</b> (0.076)
	LoL	0.850 (0.155)	0.810 (0.185)	<b>0.879</b> (0.177)	0.745 (0.137)	0.788 (0.086)	0.798 (0.158)	<u>0.858</u> (0.176)
LOE	IEC	479.804 (175.894)	218.767 (69.464)	<u>166.566</u> (68.206)	756.912 (268.587)	857.026 (354.867)	164.628 (94.176)	<b>161.478</b> (58.791)
	LoL	440.257 (133.562)	313.231 (95.686)	<b>249.241</b> (95.322)	740.402 (257.442)	893.308 (302.028)	387.972 (142.748)	<u>279.643</u> (104.040)
PSNR	IEC	17.749 (4.803)	17.303 (4.106)	<u>19.360</u> (5.491)	14.306 (2.792)	14.727 (2.710)	14.256 (3.660)	<b>20.508</b> (4.881)
	LoL	16.208 (4.549)	11.556 (3.891)	15.183 (5.568)	10.415 (3.186)	<b>17.027</b> (3.081)	14.024 (3.978)	<u>16.904</u> (4.907)

adopted for reference IQA. Greater values of MSSIM and PSNR, or smaller LOE will be better.

We used several synthesized images for experiments with various methods, including the AGCWD [54], SRIE [31], IBOOST [55], L2UWE [56], RetinexNet [58], FCCE [59] and our method, respectively. The comparison data based on these images of Fig. 17 are shown in Table 2, in which the best result is bolded and the second best one is underlined. Our approach achieves the six best values of nine and the IBOOST method obtains the rest three best values. Comparing the visual perception of Figs. 16 and 17, it is easy to find that the conclusion of objective evaluation is consistent with that of subjective visual evaluation. To make the test more general, the IEC database and LoL database is also employed for objective evaluation with the metrics of MSSIM, LOE, and PSNR. From the data in Table 3, the method proposed in this paper is shown to achieve all best performance with the above three metrics on the IEC database and three second-best values on the LoL database, while the IBOOST obtained the two best performance on the LoL database. This means that the conclusions drawn from Tables 2 and 3 are roughly the same, i.e., our method outperforms comprehensive performance over that of others.

In Tables 1 and 3, numbers in parenthesis are standard deviation. Compared to the state-of-the-art methods, the standard deviation of our method is comparable or better. That is, our method is equally consistent, and the performance gain is not a compromise of stability.

### (3) Computational complexity

To compare the processing speed of various methods, we use different sizes of images to carry out experiments in MATLAB. The average time needed for 20 operations on the same image size is taken as the runtime of that size image, which is expressed by the following formula:

$$\bar{H} = \sum_{i=1}^n H_i, \quad (19)$$

where  $n$  is sample quantity and  $H_i$  is the runtime of an image with a fixed size.

Shown as in Table 4, SRIE has the lowest efficiency in processing a single image, as it takes 242.02 s to process images of  $2048 \times 1536$  pixels [67]. However, CVC [18], MSRCP [28], DCP [37], EFF [68], NPE [30], and the method in this paper take similar amounts of time. The runtime of the MSRCP method increases rapidly with increasing

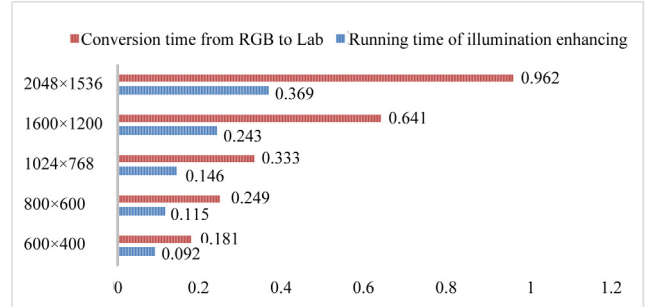


Fig. 20. Runtime comparison of different steps in the proposed method.

image size, while that of other methods increases approximately linearly with increasing image size. Among them, the proposed method has the shortest runtime and thus has lower time complexity.

After testing and analysis, most time consumed by our method mainly occurs in the process of converting from RGB to Lab color space. As shown in Fig. 20, the red column is the conversion time from RGB to Lab color space, and the blue column corresponds to the time consumed by enhancement operations. From these columns, it can be seen that it takes 0.181 s and 0.092 s to process  $600 \times 400$  pixel images, respectively, while it takes 0.962 s and 0.369 s to process  $2048 \times 1536$  pixel images, respectively. With the increase in the size of the images, the time-consuming proportion of image space conversion increases. Therefore, identifying a fast method for converting RGB to Lab color space will further improve the computational speed of the proposed method.

We find that the results of our method matched well with human subjective opinions of image quality, and are statistically superior to the other methods.

### 4.3. Adaptivity analysis

Additionally, experiments are carried out using the proposed method on images with complex illumination and images under normal illumination. The samples are shown in Fig. 21. The first row

**Table 4**

Comparison of the computational complexity (Unit: Seconds).

Method	Resolution				
	400 × 600 pixels	600 × 800 pixels	768 × 1024 pixels	1200 × 1600 pixels	1536 × 2048 pixels
CVC	0.27	0.40	0.60	1.27	2.33
MSRPC	<u>0.17</u>	0.40	0.88	3.29	7.41
DCP	0.33	0.60	1.06	2.42	3.89
SRIE	7.08	13.61	22.38	101.91	242.02
EFF	0.42	0.62	0.94	1.86	3.03
NPE	6.92	13.27	21.33	52.29	89.93
Our method	0.27	<u>0.36</u>	<u>0.48</u>	<u>0.88</u>	<u>1.33</u>



(a) Enhancement of images under complex illumination conditions



(b) Enhancement of images under normal illumination conditions



(c) Enhancement of nighttime hazy images

Fig. 21. Examples of image enhancement under different illumination conditions.

contains the low-light images, while the second row contains the improved images. Although the enhancement effect of this method is unsatisfactory, there is no block effect or noise in the restored image, which is consistent with human visual perception. The third and fourth rows are normal illumination images and the enhancement results, respectively. For the normal illumination image, the processing result of the proposed method is nearly unchanged from the original image. Fig. 21(c) shows the enhancement of haze images at night. It can be seen that this method can enhance the details of low illumination, but due to the large gray value of the haze image, the contrast will be reduced after enhancement. Therefore, only the algorithm combined with defogging can achieve satisfactory results. Overall, the proposed method can adaptively adjust parameters to different scenes and has excellent robustness and adaptability.

#### 4.4. Failure cases

In the experiment, there will be a slight over-enhancement of the bright areas in the image. Some samples are shown in Fig. 22. It

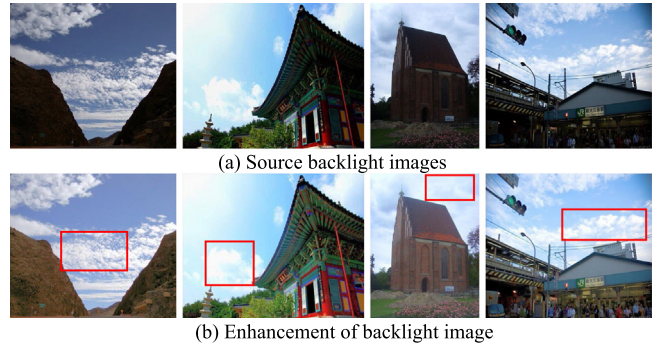


Fig. 22. Examples of backlight image enhancement.

can be seen that for images with outdoor sky areas, it is easy to enhance the white clouds, resulting in the weakening of the sky color. This is mainly because the backlight shooting results in the brightness deviation between bright and dark areas of the image. How to enhance backlight image better is still a challenging problem.

## 5. Conclusions

In this paper, we focus on addressing the issues of over-enhancement due to non-uniform illumination and the lack of self-adaptability in parameter configurations during the process of low-light images enhancement. Based on the Weber–Fechner law and a logarithmic transformation, an adaptive enhancement method for color images is put forward. After the source RGB color image is converted into Lab color space and the illumination component is extracted from the scene using the Gaussian filter function. The image is logarithmically transformed by adaptively adjusting the parameters of the illumination distribution to enhance the image brightness. Finally, the saturation of the color image is compensated. Because this algorithm dynamically adjusts the parameters of logarithmic transformation by using the illumination distribution from the scene, it plays a significant role in improving the visual quality of the image and finding details of low-light areas. Compared with the existing methods, the proposed algorithm can adaptively and quickly enhance images with complex illumination, and the enhanced image is natural. This method can be applied to video surveillance, scene restoration, and other fields and can provide a reference for image defogging and underwater image enhancement. However, the converting color space conversion of RGB and Lab will take most of the running time of the whole method, how to reduce and improve the efficiency of this process will be the research focus in the future.

## CRediT authorship contribution statement

**Wencheng Wang:** Conception or design of the work, Acquisition, Analysis, or interpretation of data for the work. **Zhenxue Chen:** Writing – original draft, Writing – review & editing. **Xiaohui Yuan:** Polished the paper including language, grammar, etc.

## Declaration of competing interest

The authors declare that they have no known competing financial interests or personal relationships that could have appeared to influence the work reported in this paper.

## Acknowledgments

This work was supported by Science and Technology Plan for Youth Innovation of Science and Technology Plan for Youth Innovation of Shandong's Universities (No. 2019KJN012), Shandong Provincial Natural Science Foundation (Nos. ZR2020KF033, ZR2019FM059), Weifang Science and technology development plan (No. 2021GX006), National Natural Science Foundation of China (Grant No. 61403283). All the authors have approved the final version to be published.

## References

- [1] M. Li, J. Liu, W. Yang, X. Sun, Z. Guo, Structure-revealing low-light image enhancement via robust retinex model, *IEEE Trans. Image Process.* 27 (6) (2018) 2828–2841.
- [2] A. Rayan, Tekli, Low-light homomorphic filtering network for integrating image enhancement and classification, *Signal Process., Image Commun.* 100 (2022) 116527.
- [3] Y. Zhu, X. Fu, A. Liu, Learning dual transformation networks for image contrast enhancement, *IEEE Signal Process. Lett.* 27 (2020) 1999–2003.
- [4] W. Wang, X. Yuan, X. Wu, Y. Liu, Fast image dehazing method based on linear transformation, *IEEE Trans. Multimedia* 19 (6) (2017) 1142–1155.
- [5] M. Veluchamy, A.K. Bhandari, B. Subramani, Optimized bezier curve based intensity mapping scheme for low light image enhancement, *IEEE Trans. Emerg. Top. Comput. Intell.* (2021) <http://dx.doi.org/10.1109/TETCI.2021.3053253>.
- [6] C. Guo, C. Li, J. Guo, et al., Zero-reference deep curve estimation for low-light image enhancement, in: Proceedings of the IEEE/CVF Conference on Computer Vision and Pattern Recognition, 2020.
- [7] M. Oloyede, G. Hancke, H. Myburgh, A. Onumanyi, A new evaluation function for face image enhancement in unconstrained environments using metaheuristic algorithms, *EURASIP J. Image Video Process.* 2019 (1) (2019) 27.
- [8] G. Hou, Z. Pan, B. Huang, G. Wang, X. Luan, Hue preserving-based approach for underwater colour image enhancement, *IET Image Process.* 12 (2) (2018) 292–298.
- [9] W. Wang, B. Xin, N. Deng, J. Li, N. Liu, Single vision based identification of yarn hairiness using adaptive threshold and image enhancement method, *Measurement* 128 (2018) 220–230.
- [10] T.A. Soomro, T.M. Khan, M.A.U. Khan, J. Gao, M. Paul, L. Zheng, Impact of ICA-based image enhancement technique on retinal blood vessels segmentation, *IEEE Access* 6 (2018) 3524–3538.
- [11] S. Pei, C. Shen, Color enhancement with adaptive illumination estimation for low-backlighted displays, *IEEE Trans. Multimedia* 19 (8) (2017) 1956–1961.
- [12] F. Kallel, M. Sahnoun, A.B. Hamida, K. Chtourou, Ct scan contrast enhancement using singular value decomposition and adaptive gamma correction, *Signal Image Video Process.* 12 (5) (2018) 905–913.
- [13] F. Drago, K. Myszkowski, T. Annen, N. Chiba, Adaptive logarithmic mapping for displaying high contrast scenes, *Comput. Graph. Forum* 22 (3) (2003) 419–426.
- [14] S. Huang, F. Cheng, Y. Chiu, Efficient contrast enhancement using adaptive gamma correction with weighting distribution, *IEEE Trans. Image Process.* 22 (3) (2013) 1032–1041.
- [15] W. Wang, X. Yuan, Z. Chen, X. Wu, Z. Gao, Weak-light image enhancement method based on adaptive local gamma transform and color compensation, *J. Sensors* (2021).
- [16] T.K. Kim, J.K. Paik, B.S. Kang, Contrast enhancement system using spatially adaptive histogram equalization with temporal filtering, *IEEE Trans. Consum. Electron.* 44 (1) (1998) 82–87.
- [17] Y.T. Kim, Contrast enhancement using brightness preserving bi-histogram equalization, *IEEE Trans. Consum. Electron.* 43 (1) (1997) 1–8.
- [18] T. Celik, T. Tjahjadi, Contextual and variational contrast enhancement, *IEEE Trans. Image Process.* 20 (12) (2011) 3431–3441.
- [19] A.S. Parihar, O.P. Verma, Contrast enhancement using entropy-based dynamic sub-histogram equalisation, *IET Image Process.* 10 (11) (2016) 799–808.
- [20] K. Gu, G. Zhai, W. Lin, M. Liu, The analysis of image contrast: From quality assessment to automatic enhancement, *IEEE Trans. Cybern.* 46 (1) (2016) 284–297.
- [21] H. Xu, G. Zhai, X. Wu, X. Yang, Generalized equalization model for image enhancement, *IEEE Trans. Multimedia* 16 (1) (2014) 68–82.
- [22] X. Zong, A.F. Laine, E.A. Geiser, Speckle reduction and contrast enhancement of echocardiograms via multiscale nonlinear processing, *IEEE Trans. Med. Imaging* 17 (4) (1998) 532–540.
- [23] A. Loza, D.R. Bull, P.R. Hill, A.M. Achim, Automatic contrast enhancement of low-light images based on local statistics of wavelet coefficients, *Digit. Signal Process.* 23 (6) (2013) 1856–1866.
- [24] E.H. Land, J.J. McCann, Lightness and retinex theory, *J. Opt. Soc. Amer.* 61 (1) (1971) 1–11.
- [25] D.J. Jobson, Z. Rahman, G.A. Woodell, Properties and performance of a center/surround retinex, *IEEE Trans. Image Process.* 6 (3) (1997) 451–462.
- [26] D.J. Jobson, Z. Rahman, G.A. Woodell, A multiscale retinex for bridging the gap between color images and the human observation of scenes, *IEEE Trans. Image Process.* 6 (7) (2002) 965–976.
- [27] Z. Rahman, D. Jobson, G. Woodell, Retinex processing for automatic image enhancement, *J. Electron. Imag.* 13 (1) (2004) 100–110.
- [28] A.B. Petro, C. Shert, J.M. Morel, Multiscale retinex, image process, Line 4 (2014) 71–88.
- [29] J.H. Jang, Y. Bae, J.B. Ra, Contrast-enhanced fusion of multisensor images using subband-decomposed multiscale retinex, *IEEE Trans. Image Process.* 21 (8) (2012) 3479–3490.
- [30] S. Wang, J. Zheng, H.M. Hu, B. Li, Naturalness preserved enhancement algorithm for non-uniform illumination images, *IEEE Trans. Image Process.* 22 (9) (2013) 3538–3548.
- [31] X. Fu, D. Zeng, Y. Huang, X. Zhang, X. Ding, A weighted variational model for simultaneous reflectance and illumination estimation, in: 2016 IEEE Conf. Comput. Vision Pattern Recognit. (CVPR), 2016, pp. 2782–2790.
- [32] Y. Gao, H. Hu, B. Li, Q. Guo, Naturalness preserved non-uniform illumination estimation for image enhancement based on retinex, *IEEE Trans. Multimedia* (2) (2018) 335–344.
- [33] J. Xiao, S. Shan, P. Duan, T. Chao-Ping, Y. Ben-Shun, A fast image enhancement algorithm based on fusion of different color spaces, *Acta Automat. Sinica* 40 (4) (2014) 697–705.
- [34] J. Wei, Q. Zhijie, X. Bo, Z. Dean, A nighttime image enhancement method based on retinex and guided filter for object recognition of apple harvesting robot, *Int. J. Adv. Rob. Syst.* 15 (1) (2018) 172988141775387.
- [35] X. Kong, L. Liu, Y. Qian, Low-light image enhancement via Poisson noise aware retinex model, *IEEE Signal Process. Lett.* (28) (2021) 1540–1544.
- [36] Xutong Ren, et al., Lr3 m: Robust low-light enhancement via low-rank regularized retinex model, *IEEE Trans. Image Process.* 29 (2020) 5862–5876.
- [37] X. Dong, G. Wang, Y. Pang, W. Li, J. Wen, W. Meng, et al., Fast efficient algorithm for enhancement of low lighting video, in: 2011 IEEE Int. Conf. Multimedia Expo, 2011, pp. 1–6.
- [38] X. Zhang, P. Shen, L. Luo, L. Zhang, J. Song, Enhancement and noise reduction of very low light level images, in: Proc. 21st Int. Conf. Pattern Recognit. (ICPR2012), 2012, pp. 2034–2037.
- [39] X. Jiang, H. Yao, S. Zhang, X. Lu, W. Zeng, Night video enhancement using improved dark channel prior, in: 2013 IEEE Int. Conf. Image Process., 2013, pp. 553–557.
- [40] J. Pang, S. Zhang, W. Bai, A novel framework for enhancement of the low lighting video, in: 2017 IEEE Symp. Comput. Commun. (ISCC), 2017, pp. 1366–1371.
- [41] L. Zhang, P. Shen, X. Peng, G. Zhu, J. Song, W. Wei, et al., Simultaneous enhancement and noise reduction of a single low-light image, *IET Image Process.* 10 (11) (2016) 840–847.
- [42] L. Tao, C. Zhu, J. Song, T. Lu, H. Jia, X. Xie, Low-light image enhancement using CNN and bright channel prior, in: 2017 IEEE Int. Conf. Image Process. (ICIP), 2017, pp. 3215–3219.
- [43] S. Park, B. Moon, S. Ko, S. Yu, J. Paik, Low-light image restoration using bright channel prior-based variational retinex model, *EURASIP J. Image Video Process.* 2017 (1) (2017) 44, 2017/06/30.
- [44] Y. Hu, Y. Shang, X. Fu, Low-illumination video enhancement algorithm based on combined atmospheric physical model and luminance transmission map, *J. Image Graph.* 21 (8) (2016) 1010–1020.
- [45] J. Cepeda-Negrete, R.E. Sanchez-Yanez, Automatic selection of color constancy algorithms for dark image enhancement by fuzzy rule-based reasoning, *Appl. Soft Comput.* 28 (2015) 1–10.
- [46] K.G. Lore, A. Akintayo, S. Sarkar, LLNet: A deep autoencoder approach to natural low-light image enhancement, *Pattern Recognit.* 61 (2017) 650–662.
- [47] L. Shen, Z. Yue, F. Feng, Q. Chen, S. Liu, J. Ma, MSR-net: Low-light image enhancement using deep convolutional network, 2017, [arXiv:1711.02488](https://arxiv.org/abs/1711.02488).
- [48] L. Tao, C. Zhu, G. Xiang, Y. Li, H. Jia, X. Xie, LLCNN: A convolutional neural network for low-light image enhancement, in: 2017 IEEE Vis. Commun. Image Process. (VCIP), 2017, pp. 1–4.
- [49] S. Park, S. Yu, M. Kim, K. Park, J. Paik, Dual autoencoder network for retinex-based low-light image enhancement, *IEEE Access* 6 (2018) 22084–22093.

- [50] J. Cai, S. Gu, L. Zhang, Learning a deep single image contrast enhancer from multi-exposure images, *IEEE Trans. Image Process.* 27 (4) (2018) 2049–2062.
- [51] M. Gharbi, J. Chen, J.T. Barron, S.W. Hasinoff, F. Durand, Deep bilateral learning for real-time image enhancement, *ACM Trans. Graph. (TOG)* 36 (4) (2017) 118.
- [52] W. Wang, C. Wei, W. Yang, J. Liu, GLADNet: Low-light enhancement network with global awareness, in: 2018 13th IEEE Int. Conf. Automat. Face Gesture Recognit. (FG 2018), 2018, pp. 751–755.
- [53] J. Shen, On the foundations of vision modeling III. Noncommutative monoids of occlusive preimages, *J. Math. Img. Vis.* 24 (1) (2006) 5–17.
- [54] S. Huang, C. Cheng, Y. Chiu, Efficient contrast enhancement using adaptive gamma correction with weighting distribution, *IEEE Trans. Image Process.* 22 (3) (2013) 1032–1041.
- [55] A. Zohair, Nighttime image enhancement using a new illumination boost algorithm, *IET Image Process.* 13 (8) (2019) 1314–1320.
- [56] T. Marques, A. Albu, L<sup>2</sup>UWE: A framework for the efficient enhancement of low-light underwater images using local contrast and multi-scale fusion, in: *IEEE Conf. Comput. Vision Pattern Recognit. (CVPR)*, 2020, pp. 538–539.
- [57] Y. Zhang, J. Zhang, X. Guo, Kindling the darkness: a practical low-light image enhancer, 2019, arXiv:1905.04161.
- [58] C. Wei, W. Wang, W. Yang, J. Liu, Deep retinex decomposition for low-light enhancement, in: *The British Machine Vision Conference*, 2018.
- [59] A. Parihar, O. Verma, C. Khanna, Fuzzy-contextual contrast enhancement, *IEEE Trans. Image Process.* 26 (4) (2017) 1810–1819.
- [60] S. Cristiano, L. Paulo, S. Silvia, Deep learning based exposure correction for image exposure correction with application in computer vision for robotics, in: *2018 Latin American Robotic Symposium*, 2018.
- [61] L. Ying, Z. Li, C. Zhang, No-reference sharpness assessment with fusion of gradient information and HVS filter, *J. Image Graph.* 20 (11) (2015) 1446–1452.
- [62] A. Mittal, R. Soundararajan, A. Bovik, Making a completely blind image quality analyzer, *IEEE Signal Process. Lett.* 20 (3) (2013) 209–212.
- [63] C. Lee, C. Lee, C. Kim, Contrast enhancement based on layered difference representation of 2D histograms, *IEEE Trans. Image Process.* 22 (12) (2013) 5372–5384.
- [64] P. Tian, W. Shuhang, Perceptually motivated enhancement method for non-uniformly illuminated images, *IET Comput. Vis.* 12 (4) (2018) 424–433.
- [65] Z. Wang, E.P. Simoncelli, A.C. Bovik, Multi-scale structural similarity for image quality assessment, in: *Invited Paper, IEEE Asilomar Conference on Signals, Systems and Computers*, 2003.
- [66] S. Wang, J. Zheng, H. Hu, B. Li, Naturalness preserved enhancement algorithm for non-uniform illumination images, *IEEE Trans. Image Process.* 22 (9) (2013) 3538–3548.
- [67] W. Wang, Z. Chen, X. Yuan, X. Wu, Adaptive image enhancement method for correcting low-illumination images, *Inform. Sci.* 496 (2019) 25–41.
- [68] Z. Ying, G. Li, Y. Ren, R. Wang, W. Wang, A new image contrast enhancement algorithm using exposure fusion framework, in: *Int. Conf. Comput. Anal. Images Patterns*, 2017, pp. 36–46.